SUPPORTING INFORMATION

Single-Atom Imino Substitutions at A9 and A10 Reveal Distinct Effects on the Fold and Function of the Hairpin Ribozyme Catalytic Core[†]

Robert C. Spitale[‡], Rosaria Volpini[§], Michael V. Mungillo[‡], Jolanta Krucinska[‡], Gloria Cristalli[§] and Joseph E. Wedekind[‡,*]

[‡]Department of Biochemistry & Biophysics, 601 Elmwood Avenue Box 712, Rochester New York 14642, [§]Department of Chemical Sciences, University of Camerino, Via S. Agostino 1, 62032 Camerino, Italy

[†]Support from the National Institutes of Health (NIH) grant R01 GM63162 and the donors of the Petroleum Research Fund (45534 AC4) to JEW is gratefully acknowledged. RCS was supported in part by an Elon Huntington Hooker graduate fellowship.

*To whom correspondence should be addressed. Phone: (585) 273-4516. Fax: (585) 275-6007. E-mail: joseph.wedekind@rochester.edu

RNA constructs used in this study: The minimal form of the hairpin ribozyme utilized in this study (Figure S1) was described previously (*1*). The 19-mer ribozyme strand and 13-mer substrate strand were synthesized by Dharmacon Inc. (Fayette, CO). The 29-mer strand containing a 10-atom linker with N1dA or adenosine at positions 9 and 10 was synthesized by Dharmacon Inc. (Fayette, CO). The 13-mer 2′,5′-linked strand (transition-state analogue) was synthesized by Fidelity Systems Inc (Gaithersburg, MD) utilizing a 2′,5′-linked, 3′-deoxy phosphoramidite from Glen Research (Sterling, VA) as described (*2, 3*). Each of the synthesized RNA strands was deprotected as per manufacturers' instructions, purified by HPLC, and desalted as described previously (*4*).

Crystallization, X-Ray diffraction, and structural solution experiments*:* Each of the RNA strands was combined and docked as described (*2, 5*). Crystals were grown from hanging-drop vapor-diffusion at 20 ^{o}C. Well solutions contained 20.5% (w/v) PEG 2K MME, 0.10 M Na-Cacodylate (pH = 6.5 or 7.0), 0.25 M Li_2SO_4, 2.5 mM $Co(NH_3)_6Cl_3$ and 2 mM spermidine-HCl. Crystals grew as hexagonal rods or plates and reached a size of 0.3 mm x 0.2 mm x 0.2 mm in approximately 3 weeks. Each crystal was cryoprotected by serial transfer into glycerol and frozen by plunging into $N_2(l)$. The crystals were loaded into a cassette (Crystal Positioning Systems) and shipped to the Stanford Synchrotron Radiation Laboratory for remote data collection on the Stanford Automounting System at beamline 7–1 using Blu-Ice and Web-Ice interfaces (*6*). 120 images for each crystal were collected at a crystal-to-detector distance of 15.0 cm with 20 min exposures and $\Delta\Phi$ = 0.5° per oscillation using a Quantum 315 CCD detector (ADSC). Intensity data were reduced using the HKL2000 suite with intensity statistics provided in Table S1. Each structure was solved by difference Fourier methods using a previously determined pre-catalytic structure to 2.05 Å resolution (PDB 2OUE) as a starting model. Maximum likelihood refinement was used throughout as described (*1*).

Activity Assays: Single-turnover cleavage assays were performed using a 13-

mer substrate strand that was ^{32}P labeled as described (*1*). The fraction of substrate cleaved relative to input substrate was quantified using *ImageQuant* software (Molecular Dynamics). Experimental data from the time-dependent cleavage assays were fitted to a double-exponential equation: $F(t) = A_0 + A_1[1 - \exp - k_1 t] + A_2[1 - \exp - k_2 t]$, where A_1 and A_2 represent amplitudes for the reactive fraction of HPRZ in the biphasic time course. The values k_1 and k_2 are the corresponding first-order rate constants of the fast and slow phases, respectively, and t is time. A_0 represents the initial amount cleaved, which was about 3%. Amplitudes and rate constants were derived from a Marquardt-Levenberg nonlinear least-squares regression routine (*SigmaPlot* 9.0). Detailed methods have been described elsewhere [refs. (*7-10*)]. The fast phase amplitudes for WT, N1dA9 and N1dA10 were: 0.47, 0.26 and 0.45. The respective fast-phase (k_1) rate constants were: 0.84 min^{-1} ± 0.05 min^{-1}, 0.12 min^{-1} ± 0.02 $min^{-1}$and 0.96 min^{-1} ± 0.04 min^{-1}. The respective slow-phase (k_2) rate constants were: 0.010 min^{-1} ± 0.002 min^{-1} , 0.015 min^{-1} ± 0.003 min^{-1} and 0.020 min^{-1} ± 0.003 min^{-1}.

Table S1: X-ray Diffraction Data and Refinement Statistics

	N1dA9 2'OMe	N1dA9 2',5'	N1dA1- 2'OMe	N1dA10 2',5'
PDB code:	3I2Q	3I2R	3I2S	3I2U
Space group:	$P6_122$	$P6_122$	$P6_122$	$P6_122$
Unit cell (Å):	a = 93.3	a = 93.6	a = 92.8	a = 94.1
	c = 131.4	c = 132.2	c = 132.7	c = 134.5
Resolution:	2.90	2.80	2.75	2.80
(Å)[a]:	(3.0-2.90)	(2.90-2.80)	(2.85-2.75)	(2.90-2.80)
Mosaicity (°):	1.16	1.12	1.18	1.078
no. Unique flections:	9,310	8,903	9,249	11,339
Total No. reflections:	62,716	83,774	64,743	167,957
Redundancy[a]:	7.8 (7.1)	9.4(10.5)	7.1(7.1)	13.01(13.49)
Completeness (%)[a]:	99.6 (99.8)	99.5(100.0)	99.3(100.0)	99.6(100.0)
$I/\sigma(I)$[a]:	27.4(1.8)	13.1(3.7)	52.2(3.5)	16.9(3.1)
R_{sym} (%)[a,b]:	7.7(46.4)	8.1(45.4)	6.8(49.9)	6.8(42.7)
No. RNA atoms[c]:	1312	1310	1312	1310
No. ions:	$2Co(NH_3)_6$(III) $1SO_4^{2-}$	$2Co(NH_3)_6$(III) $1SO_4^{2-}$	$2Co(NH_3)_6$(III) $1SO_4^{2-}$	$2Co(NH_3)_6$(III) $1SO_4^{2-}$
Average B-factor (Å^2):	73.0	69.1	72.4	70.8
R_{cryst}	20.5	23.7	23.0	24.9
R_{work}/R_{free} (%)[d,e]:	20.3/22.7	23.2/27.3	23.9/26.1	24.4/26.6
rmsd bonds (Å)	0.006	0.008	0.006	0.009
rmsd angles (°):	1.4	1.6	1.6	1.7
Coord. error (Å):	0.48	0.49	0.57	0.51

[a]Values referring to the highest resolution shell are in parentheses.
[b]$R_{sym} = \Sigma_{hkl}|I_j - \langle I_j \rangle|/\Sigma_{hkl}|I_j| \times 100$.
[c]Number of RNA atoms includes dual conformations for U-5, but not atoms of the linker.
[d] $R_{cryst} = \Sigma_{hkl}|F_o - kF_c|/\Sigma_{hkl}|F_o| \times 100$, where k is a scale factor.
[e]R_{free} is defined as the R_{cryst} calculated using 7.4% of data excluded from refinement.
[f]Based upon the cross-validated Luzzati plots calculated for the full resolution range.

References:

1. Spitale, R. C., and Wedekind, J. E. (2009) *Methods*, doi:10.1016/j.ymeth. 2009.1006.1003
2. Torelli, A. T., Krucinska, J., and Wedekind, J. E. (2007) *RNA 13*, 1052-1070.
3. Torelli, A. T., Spitale, R. C., Krucinska, J., and Wedekind, J. E. (2008) *Biochem Biophys Res Commun 371*, 154-158.
4. Wedekind, J. E., and McKay, D. B. (2000) *Methods Enzymol. 317*, 149-168.
5. Alam, S., Grum-Tokars, V., Krucinska, J., Kundracik, M. L., and Wedekind, J. E. (2005) *Biochemistry 44*, 14396-14408.
6. McPhillips, T. M., McPhillips, S. E., Chiu, H. J., Cohen, A. E., Deacon, A. M., Ellis, P. J., Garman, E., Gonzalez, A., Sauter, N. K., Phizackerley, R. P., Soltis, S. M., and Kuhn, P. (2002) *J Synchrotron Radiat 9*, 401-406.
7. Esteban, J. A., Banerjee, A. R., and Burke, J. M. (1997) *J Biol Chem 272*, 13629-13639.
8. Esteban, J. A., Walter, N. G., Kotzorek, G., Heckman, J. E., and Burke, J. M. (1998) *Proc Natl Acad Sci U S A 95*, 6091-6096.
9. MacElrevey, C., Spitale, R. C., Krucinska, J., and Wedekind, J. E. (2007) *Acta Crystallogr. D Biol. Crystallogr. 63*, 812-825.
10. Rueda, D., Bokinsky, G., Rhodes, M. M., Rust, M. J., Zhuang, X., and Walter, N. G. (2004) *Proc. Natl. Acad. Sci. U.S.A. 101*, 10066-10071.

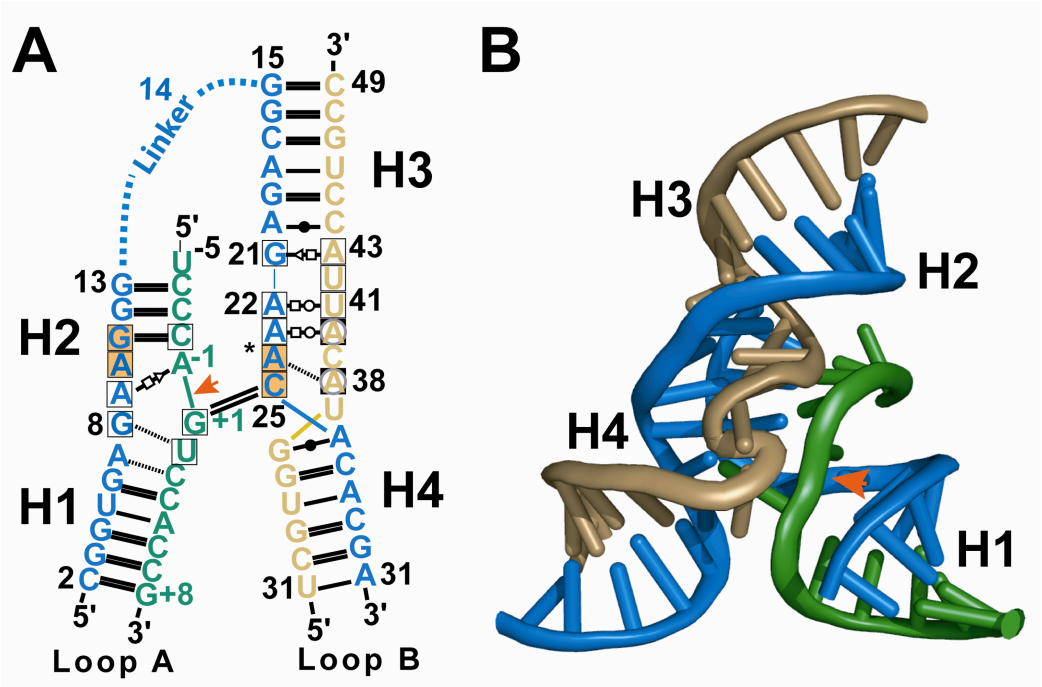

Figure S1: Representation of the linked ribozyme construct used in this study. (A) Secondary structure of the minimal, hinged hairpin ribozyme. The substrate strand is depicted in green, the S-turn strand is tan and the 29-mer strand is blue. Conserved residues are boxed; orange backgrounds indicate residues of the ribose zipper, white boxes indicate E-loop residues and circled gray residues belong to the S-turn. Hydrogen-bond pairings: open-square, Hoogsteen; open triangle, trans-sugar; open circle, Watson–Crick face; closed circle, wobble pair. Double and single lines indicate Watson–Crick pairs; black dashed lines indicate single hydrogen bonds. An arrow indicates the scissile bond. (B) Cartoon diagram of the minimal, hinged hairpin ribozyme structure, colored as in (A).

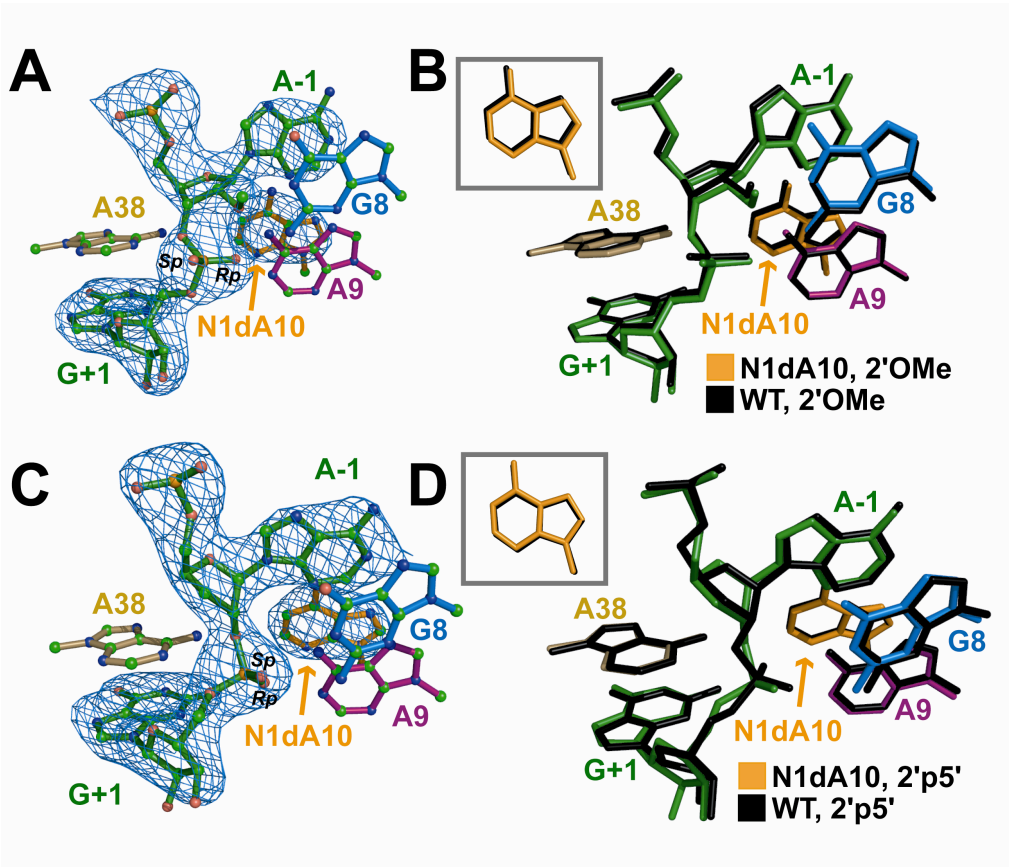

Figure S2: Structural representations of the N1dA10 strands evaluated in this study. (A) The N1dA10 variant in the context of the pre-catalytic construct. The simulated-annealing-omit electron-density map at 2.75 Å resolution is contoured at the 3σ level. (B) The pre-catalytic N1dA9 variant superimposed on the WT structure (PDB 2OUE). (C) The N1dA10 variant in the context of 2′,5′-linkage TSA. The simulated-annealing-omit electron-density map at 2.80 Å resolution is contoured at the 3σ level. (D) The N1dA10 variant in the context of the 2′,5′-TSA superimposed on a matched WT structure (PDB 2P7F).

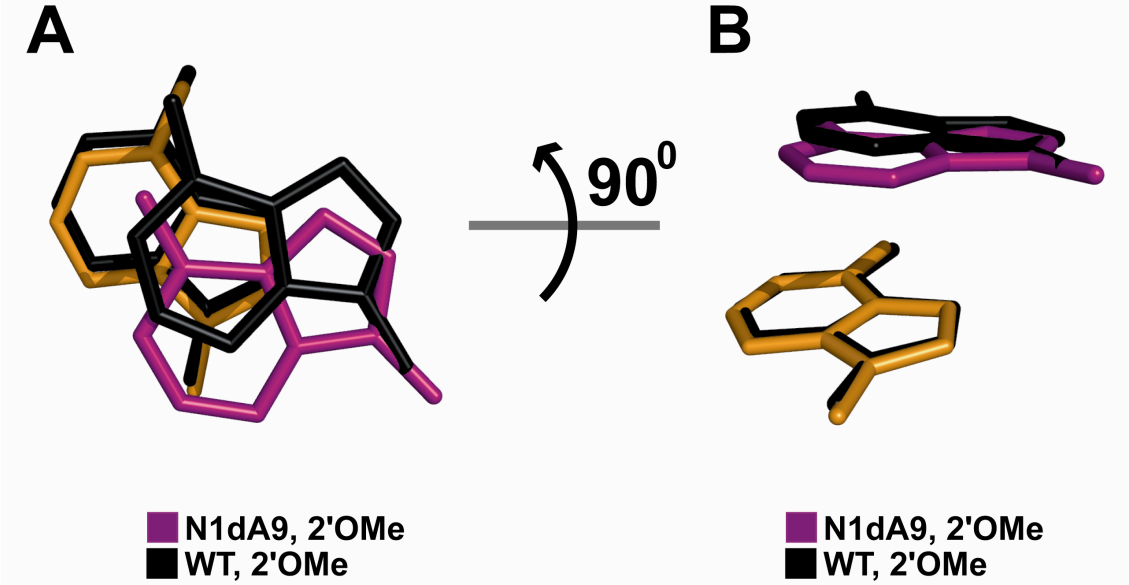

Figure S3: The experimentally observed orientation of N1dA9 in the context of a 2´-*O*-methyl 13-mer substrate strand representative of the pre-catalytic state. (A) The spatial relationship between N1dA9 and A10 shows the pyrimidine portion of of the N1dA9 bases recoiled, which decreases overlap with the imidazolium ring of A10. (B) The orientation from (A) rotated by 90^{o} about the *x*-axis.